Hindawi Publishing Corporation
Shock and Vibration
Volume 2016, Article ID 2787524, 10 pages
http://dx.doi.org/10.1155/2016/2787524

Research Article

Dynamics Analysis of Unbalanced Motorized Spindles Supported on Ball Bearings

Junfeng Liu,[1] Tao Lai,[1] and Xiaoan Chen[2]

[1]*College of Mechatronic Engineering and Automation, National University of Defense Technology, Changsha 410073, China*
[2]*The State Key Laboratory of Mechanical Transmission, Chongqing University, Chongqing 400044, China*

Correspondence should be addressed to Junfeng Liu; ljf20090702122@163.com

Received 21 January 2016; Revised 1 August 2016; Accepted 16 October 2016

Academic Editor: Gianluca Gatti

This paper presents an improved dynamic model for unbalanced high speed motorized spindles. The proposed model includes a Hertz contact force model which takes into the internal clearance and an unbalanced electromagnetic force model based on the energy of the air magnetic field. The nonlinear characteristic of the model is analysed by Lyapunov stability theory and numerical analysis to study the dynamic properties of the spindle system. Finally, a dynamic operating test is carried out on a DX100A-24000/20-type motorized spindle. The good agreement between the numerical solutions and the experimental data indicates that the proposed model is capable of accurately predicting the dynamic properties of motorized spindles. The influence of the unbalanced magnetic force on the system is studied, and the sensitivities of the system parameters to the critical speed of the system are obtained. These conclusions are useful for the dynamic design of high speed motorized spindles.

1. Introduction

Due to the complexity of the reliability and performance problems caused by profound high speed effects [1–3], the machine tools capable of achieving the high speed cutting were first introduced commercially in 1980s, which lags behind the theory of high speed metal cutting by 50 years [4]. Motorized spindles are the core components of CNC machine tools and greatly improve the cutting speed, while the inevitable unbalance of the spindle system caused by unexpected errors during manufacturing and installation process strongly influences the machining productivity and finish quality of workpieces in high speed operating conditions [5–11]. Therefore, it is necessary to deeply study the dynamic properties of unbalanced machine tool motorized spindle systems. With the low-friction and the convenience in commodity standardization, ball bearings are widely used in high speed motorized spindles [12]. Bearing clearance concerns the contact state between the balls and the inner and outer rings and affects the vibration response of the rotor system [13]. Harsha presented a model for studying the structural vibrations of ball bearing-rotor systems due to radial internal clearance [14]. Sopanen and Mikkola proposed a dynamic model of a ball bearing-rotor system with six degrees of freedom to study the effects of the bearing clearance on the natural frequencies and the vibration responses of the system [15, 16]. Based on it, Gao found that appropriate negative internal clearance helps to reduce the vibration responses of the spindle and improve the stability of the system [17, 18]. Bearing preload could keep the bearing in a negative internal clearance state by eliminating the clearance, but too large preload will produce much frictional heat, leading to the rise of temperature and the decline of bearing life [19]. With the use of the Transfer Matrix Method, Jiang and Mao investigated the variable optimum preload for a machine tool spindle [20]. Alfares and Elsharkawy constructed a mathematical model based on five degrees of dynamic system to study the influences of axial preload of angular ball bearings on the vibration behavior of a grinding machine spindle and calculated the optimum initial axial preload for the system [21].

Series of researches on the dynamic performance and the optimal design method of the unbalanced rotor-ball bearing system of motorized spindles were deeply discussed in above works. Motorized spindles are equipped with built-in motors and their output ends are directly connected with tools, and

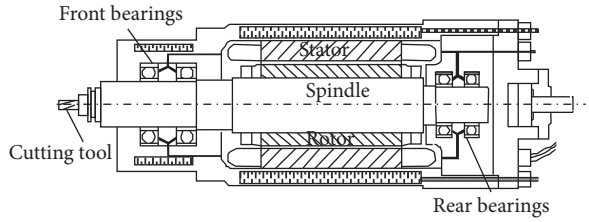

Figure 1: A typical high speed motorized spindle system.

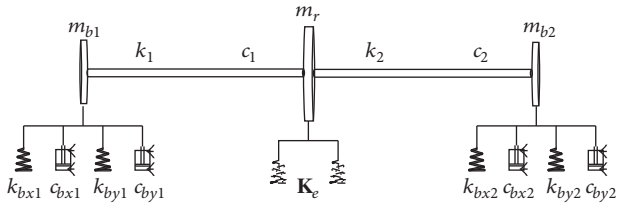

Figure 2: The simplified model of a motorized spindle system.

the rotor of the system is acted upon by an additional unbalanced magnetic force except the unbalanced centrifugal force. The unbalanced magnetic force is caused by the nonuniform air gap between the stator and the rotor in operation and affects the dynamic characteristics of the system. In view of this fact, this paper proposes the matrix expression of the magnetic stiffness based on the gap magnetic field energy. Then a dynamic model for high speed motorized spindles is established with the consideration of unbalanced magnetic force, centrifugal force, and nonlinear Hertz contact force. The vibration response and critical speed of the system are systematically calculated and experimentally validated. Finally, the sensitivities of the magnetic, mechanical, and bearing parameters to the critical speed are presented to instruct the dynamic design of unbalanced high speed motorized spindles.

2. Dynamic Model of Unbalanced Motorized Spindle System

Figure 1 shows a typical motorized spindle system which includes a stator, a spindle shaft (rotor), a cutting tool, a tool holder, and bearing components. The system can be simplified to three disc elements. Considering the motions of the discs along the vertical and horizontal directions, the spindle-bearing system is regarded as a system with six degrees of freedom, as shown in Figure 2. Specifically, the front and rear bearings are treated as springs and dampers in parallel connection, and the magnetic force is treated as springs between the stator and the rotor.

2.1. Model of Unbalance Magnetic Force. The gap eccentricity of the spindle is shown as in Figure 3, o is the inner circle center of stator (the origin of coordinates), o_1 is the outer circle center of rotor, and $|oo_1| = (x^2 + y^2)^{0.5}$. c is the centroid of rotor, e is the mass eccentricity of rotor, α is the angle between the x-axis and the circumferential position where

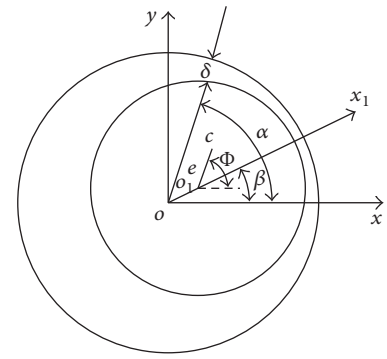

Figure 3: Air gap eccentricity of the rotor in motorized spindles.

the air gap width is equal to δ and β is the angle between the x-axis and the circumferential position where the air gap width is the least.

The built-in motor in high speed machine tool spindle system is generally a three-phase AC induction motor, so the energy of the gap magnetic field of the motor is [22]

$$W = \frac{R_g L_g}{2} \int_0^{2\pi} \Lambda_0 \sum_{n=0}^{\infty} \varepsilon^n \cos^n(\alpha - \beta) \cdot \left[F_{\mathrm{sm}} \cos\left(\omega_f t - p\alpha\right) + F_{\mathrm{rm}} \cos\left(\omega_f t - p\alpha - \varphi_1 - \varphi_2\right) \right]^2 d\alpha. \tag{1}$$

Specifically, the largest component, which is $n = 0$, plays a dominant role; other components, which are $n \neq 0$, take different proportion, respectively. Because the effective relative eccentricity ε is far less than 1, expand the high order terms in (1) and take the first three terms, and (1) can be converted into

$$W = \frac{R_g L_g \Lambda_0}{2} \int_0^{2\pi} \left(1 + \frac{x^2 + y^2}{2\sigma^2} + \frac{x}{\sigma}\cos\alpha + \frac{y}{\sigma}\sin\alpha + \frac{x^2 - y^2}{2\sigma^2}\cos 2\alpha + \frac{xy}{\sigma^2}\sin 2\alpha \right) \cdot \left[F_{\mathrm{sm}} \cos\left(\omega_f t - p\alpha\right) + F_{\mathrm{rm}} \cos\left(\omega_f t - p\alpha - \varphi_1 - \varphi_2\right) \right]^2 d\alpha, \tag{2}$$

where R_g is the radius of the inner circle of stator; L_g is effective length of rotor; Λ_0 is the magnetic conduction of uniform air gap, and $\Lambda_0 = \mu_0 / k_\mu \delta_0$, μ_0 is the air permeability, k_μ is the saturation, and $k_\mu = 1 + \delta_{\mathrm{Fe}} / k_0 \delta_0$, k_0 is the calculation coefficient of uniform air gap, δ_{Fe} is the equivalent air gap of ferromagnetic materials, δ_0 is the width of uniform air gap, $\sigma = k_\mu \delta_0$, ω_f is the speed of rotating magnetic field, and $\omega_f = 2\pi f / p$, f is the current frequency, p is the number of pole-pairs, and F_{sm} and F_{rm} are the amplitudes of three-phase resultant magnetomotive forces of the stator and the rotor, respectively; $\varphi_1 + \varphi_2$ is the phase angle in which the rotor

current lags behind the stator current, and $\varphi_1 = x_{1s}/r_1$, $\varphi_2 = x_{2s}/r_2$, x_{1s} and x_{2s} are the leakage reactance of per phase winding of the stator and the rotor, respectively; r_1 and r_2 are the resistances of per phase winding of the stator and the rotor, respectively.

Equation (2) can be expressed by

$$\mathbf{W} = \frac{1}{2}\mathbf{V}^T\mathbf{K}_e\mathbf{V} + \mathbf{V}^T\overline{\mathbf{K}_e}, \tag{3}$$

where $\mathbf{V} = \{x, y\}^T$ and $\mathbf{K}_e$ is the magnetic stiffness matrix of the gap magnetic field:

$$\begin{aligned}
K_{11} &= \frac{R_g L_g \Lambda_0}{2\sigma^2}\int_0^{2\pi}\left\{[1+\cos(2\alpha)]\right.\\
&\quad\cdot\left[F_{\mathrm{sm}}\cos\left(\omega_f t - p\alpha\right)\right.\\
&\quad\left.\left.+ F_{\mathrm{rm}}\cos\left(\omega_f t - p\alpha - \varphi_1 - \varphi_2\right)\right]^2\right\}d\alpha\\
K_{12} = K_{21} &= \frac{R_g L_g \Lambda_0}{2\sigma^2}\int_0^{2\pi}\left\{[\sin(2\alpha)]\right.\\
&\quad\cdot\left[F_{\mathrm{sm}}\cos\left(\omega_f t - p\alpha\right)\right.\\
&\quad\left.\left.+ F_{\mathrm{rm}}\cos\left(\omega_f t - p\alpha - \varphi_1 - \varphi_2\right)\right]^2\right\}d\alpha\\
K_{22} &= \frac{R_g L_g \Lambda_0}{2\sigma^2}\int_0^{2\pi}\left\{[1-\cos(2\alpha)]\right.\\
&\quad\cdot\left[F_{\mathrm{sm}}\cos\left(\omega_f t - p\alpha\right)\right.\\
&\quad\left.\left.+ F_{\mathrm{rm}}\cos\left(\omega_f t - p\alpha - \varphi_1 - \varphi_2\right)\right]^2\right\}d\alpha.
\end{aligned} \tag{4}$$

$\overline{\mathbf{K}_e}$ is the vector of the gap magnetic field energy:

$$\begin{aligned}
\overline{K_1} &= \frac{R_g L_g \Lambda_0}{2\sigma^2}\int_0^{2\pi}\left\{\cos\alpha\cdot\left[F_{\mathrm{sm}}\cos\left(\omega_f t - p\alpha\right)\right.\right.\\
&\quad\left.\left.+ F_{\mathrm{rm}}\cos\left(\omega_f t - p\alpha - \varphi_1 - \varphi_2\right)\right]^2\right\}d\alpha\\
\overline{K_2} &= \frac{R_g L_g \Lambda_0}{2\sigma^2}\int_0^{2\pi}\left\{\sin\alpha\cdot\left[F_{\mathrm{sm}}\cos\left(\omega_f t - p\alpha\right)\right.\right.\\
&\quad\left.\left.+ F_{\mathrm{rm}}\cos\left(\omega_f t - p\alpha - \varphi_1 - \varphi_2\right)\right]^2\right\}d\alpha.
\end{aligned} \tag{5}$$

2.2. Hertz Contact Force Model of Ball Bearings. In the rotor-ball bearing system of a high speed motorized spindle, the inner and outer races of the bearings are fixed to the rotating shaft and the bearing housing, respectively. Balls can be considered to make pure rolling movement between the inner race and the outer race with equal spacing. Therefore for the ball bearing in any time, the elastic deformation associated with the contact point at the jth ball depends on the displacement of rotor and the initial bearing clearance, given by

$$\Delta_j = x_b\sin\theta_j + y_b\cos\theta_j - \gamma, \tag{6}$$

where x_b and y_b are the displacements at the bearing along x- and y-directions, respectively; θ_j is the azimuth of the jth ball, and $\theta_j = (2\pi/N_b)(j-1) + (d_i/(d_i+d_o))\omega t$, N_b is the number of balls, d_i is the inner diameter of inner race, and d_o is the outer diameter of outer race; γ is the initial bearing clearance, which can be determined according to the initial bearing preload [15].

Considering that the contact force is nonnegative, the local Hertz contact force and deflection relationship for bearing can be written as [18]

$$F_{\theta_j} = \begin{cases} k_b\cdot\Delta_j^{2/3}; & \Delta_j > 0\\ 0; & \Delta_j \le 0. \end{cases} \tag{7}$$

k_b is contact stiffness which is given as

$$k_b = \left\{\frac{1}{\left(k_i^{-1}\right)^{2/3} + \left(k_o^{-1}\right)^{2/3}}\right\}^{3/2}, \tag{8}$$

where $k_i = k_o = (2\sqrt{2}/3)\cdot(E/(1-\mu))(\Sigma\rho)^{-1/2}\cdot(\delta^*)^{-3/2}$, E is the elastic modulus, and μ is the Poisson ratio. The curvature sum $\Sigma\rho$ and deformation coefficient δ^* are obtained from Harris [23].

Similar to [24], the contact damping can be written as

$$c_b = 10^{-5}\cdot k_b. \tag{9}$$

By summing the local contact forces, the total restoring force components of the ball bearing along the x- and y-directions are given by

$$\begin{aligned}
F_{bx} &= -c_b\dot{x}_b - \sum_{j=1}^{N_b}F_{\theta_j}\sin\theta_j;\\
F_{by} &= -c_b\dot{y}_b - \sum_{j=1}^{N_b}F_{\theta_j}\cos\theta_j.
\end{aligned} \tag{10}$$

2.3. Motional Differential Equations and Stability Analysis of the Spindle System. As the middle part of the spindle system is simplified to a disc element, the gap eccentricity of the motor is considered as uniform. Without regard for the influence of gyroscopic moment, the differential equations governing motions of the motorized spindle systems can be obtained with Newton second law:

$$\begin{aligned}
&m_{b1}\ddot{x}_{b1} + c_1\left(\dot{x}_{b1} - \dot{x}_r\right) + k_1\left(x_{b1} - x_r\right) = -N_1\cdot F_{bx1}\\
&m_{b1}\ddot{y}_{b1} + c_1\left(\dot{y}_{b1} - \dot{y}_c\right) + k_1\left(y_{b1} - y_r\right) = -m_{b1}\cdot g\\
&\quad - N_1\cdot F_{by1}\\
&m_r\ddot{x}_r + c_1\left(\dot{x}_r - \dot{x}_{b1}\right) + c_2\left(\dot{x}_r - \dot{x}_{b2}\right) + k_1\left(x_r - x_{b1}\right)\\
&\quad + k_2\left(x_r - x_{b2}\right) + K_{11}\cdot x_r + K_{12}\cdot y_r = F_{cx} - \overline{K_1}\\
&m_r\ddot{y}_r + c_1\left(\dot{y}_r - \dot{y}_{b1}\right) + c_2\left(\dot{y}_r - \dot{y}_{b2}\right) + k_1\left(y_r - y_{b1}\right)\\
&\quad + k_2\left(y_r - y_{b2}\right) + K_{21}\cdot x_r + K_{22}\cdot y_r = F_{cy} - m_r\cdot g\\
&\quad - \overline{K_2}
\end{aligned}$$

$$
\begin{aligned}
&m_{b2}\ddot{x}_{b2} + c_2\left(\dot{x}_{b2} - \dot{x}_r\right) + k_2\left(x_{b2} - x_r\right) = -N_2 \cdot F_{bx2} \\
&m_{b2}\ddot{y}_{b2} + c_2\left(\dot{y}_{b2} - \dot{y}_r\right) + k_2\left(y_{b2} - y_r\right) = -m_{b2} \cdot g \\
&\quad - N_2 \cdot F_{by2},
\end{aligned} \tag{11}
$$

where x_{b1} and y_{b1}, x_r and y_r, and x_{b2} and y_{b2} are the displacements of mass elements distributed at the front bearing, rotor, and the rear bearing along x- and y-directions, respectively. It should be noticed that the variable y is defined along the opposite direction of the gravity. m_{b1}, m_r, and m_{b2} are the masses of the spindle distributed at the front bearing, middle between the two sets of bearings, and the rear bearing, respectively, k_1 and k_2 are the bending stiffness of the spindle, c_1 and c_2 are the material damping of the spindle, respectively, and $c_q = 0.001/\omega \cdot k_q$, $q = 1, 2$; N_1 and N_2 are the number of the two sets of bearings, respectively; $F_{cx} = m_r e\omega^2 \cos\phi$; $F_{cy} = m_r e\omega^2 \sin\phi$, where ω is the angular velocity of rotor, and $\omega = (1 - s)\omega_f$, s is the slip of motor, ϕ is the eccentric angle of rotor mass, and $\phi = \omega t$.

Without the influence of the unbalanced magnetic force, the values of the magnetic stiffness matrix and vector of the gap magnetic field in (11) are zero.

Equations (1), (2), (3), (6), (7), (8), (9), (10), and (11) constitute the dynamic model of the unbalanced motorized spindle system. There are coupling items in the model due to the magnetic stiffness; meanwhile the total restoring forces F_{bx}, F_{by} are nonlinear functions of vibration amplitudes in x- and y-directions, so the model has strong nonlinear characteristic and the nonlinear vibration theory must be used [25]. The state equations of (11) can be given as

$$
F = \begin{Bmatrix}
\dot{x}_{b1} \\
\dot{y}_{b1} \\
\dot{x}_r \\
\dot{y}_r \\
\dot{x}_{b2} \\
\dot{y}_{b2} \\
\dfrac{-1}{m_{b1}} \cdot \left[c_1\left(\dot{x}_{b1} - \dot{x}_r\right) + k_1\left(x_{b1} - x_r\right) + N_1 \cdot F_{bx1}\right] \\
\dfrac{-1}{m_{b1}} \cdot \left[c_1\left(\dot{y}_{b1} - \dot{y}_r\right) + k_1\left(y_{b1} - y_r\right) + m_{b1} \cdot g + N_1 \cdot F_{by1}\right] \\
\dfrac{-1}{m_r} \cdot \left[c_1\left(\dot{x}_r - \dot{x}_{b1}\right) + c_2\left(\dot{x}_r - \dot{x}_{b2}\right) + k_1\left(x_r - x_{b1}\right) + k_2\left(x_r - x_{b2}\right) + K_{11} \cdot x_r + K_{12} \cdot y_r - F_{cx} + \overline{K_1}\right] \\
\dfrac{-1}{m_r} \cdot \left[c_1\left(\dot{y}_r - \dot{y}_{b1}\right) + c_2\left(\dot{y}_r - \dot{y}_{b2}\right) + k_1\left(y_r - y_{b1}\right) + k_2\left(y_r - y_{b2}\right) + K_{21} \cdot x_r + K_{22} \cdot y_r - F_{cy} + m_r \cdot g + \overline{K_2}\right] \\
\dfrac{-1}{m_{b2}} \cdot \left[c_2\left(\dot{x}_{b2} - \dot{x}_r\right) + k_2\left(x_{b2} - x_r\right) + N_2 \cdot F_{bx2}\right] \\
\dfrac{-1}{m_{b2}} \cdot \left[c_2\left(\dot{y}_{b2} - \dot{y}_r\right) + k_2\left(y_{b2} - y_r\right) + m_{b2} \cdot g + N_2 \cdot F_{by2}\right]
\end{Bmatrix}. \tag{12}
$$

The accelerations and velocities are zero in (12) when the spindle system is in equilibrium. According to the first approximate theory of Lyapunov, the motion stability of the nonlinear system is determined by the latent root of the linear approximation system. Expand the state equation (12) at the equilibrium point approximately, and the Jacobi matrix can be obtained. If all Jacobi Matrix Eigen values have negative real parts, the system is asymptotically stable. When part of the Jacobi Matrix Eigen values own negative real parts while the others own positive real parts, the system is unstable. On the other hand, once the value of a real part of the Jacobi Matrix Eigen is zero while the others are not, the system is in a critical state and is starting buckling, and then the critical speed of the spindle could be obtained. Due to the strongly nonlinear characteristic, the equation must be solved with numerical analysis. The Runge-Kutta method is used to calculate (11) to obtain the dynamic responses of the system.

3. Experimental Setup and Measurements

3.1. Parameters. To validate the proposed dynamic model, a dynamic operating test was carried out on a DX100A-24000/20-type motorized spindle. The maximum rated speed of the spindle is 24000 rpm. Both the two sets of the bearings are a pair in bearing combination with constant preload, and the front and rear bearings are the angular contact ball bearings of 7006CYTAHQ1 and 7005CYTASP4, respectively, from HRB-BC. Table 1 lists the other parameters of the spindle system. It deserves noting that the spindle system can operate with the speed higher than the maximum rated speed in a short time, and the oil dripping rate remains constant in the test to obtain the experimental data with same parameters and conditions.

3.2. Experimental Setup. A dynamic operating test is carried out to obtain the values of vibration response at different

Table 1: Parameters of DX100A-24000/20-type motorized spindle.

Parameter	Units	Given value
m_{b1}	kg	0.212
m_{b2}	kg	0.201
m_r	kg	0.483
k_1	N/mm	12100
d_i	mm	6.35/6.70
d_o	mm	6.65/7.05
N_b		18/18
k_2	N/mm	9840
s		0.01
e	μm	0.879
R_g	mm	48
L_g	mm	45
Λ_0	H/mm^2	1.468×10^{-9}
σ	mm	0.856
F_{sm}	A	463.4
F_{rm}	A	418.3
φ_1	∘	57.2
φ_2	∘	11.3
p		1
μ		0.3
Γ	mm	−0.0012
δ_0	mm	0.97

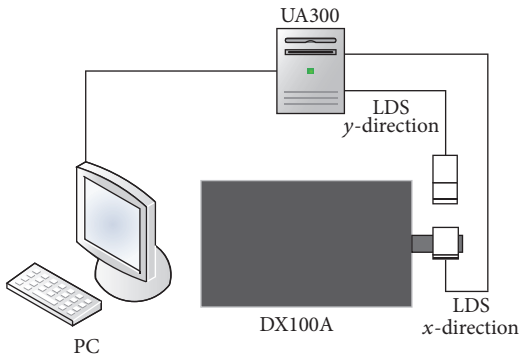

Figure 4: Experimental setup.

speeds. Due to the sharp increase of the vibratory output of the spindle system at the resonant frequency, the first critical speed of the system can be obtained from the variation of the vibration responses of the rotor. To avoid the influence of the thermal displacement, each vibration signal with a speed was collected as quickly as possible once the operating speed is stable, and the interval of each signal collection is more than half an hour.

As shown in Figure 4, the vibration signals in x- and y-directions at the front end of rotor under work conditions were acquired by using Laser Displacement Sensor (LDS), then transmitted and transformed through the signal collector and analyser UA300, and finally transmitted to the PC to be handled by the signal acquisition procedure compiled by Visual C++ 6.0.

Table 2: First critical speeds of DX100A-24000/20-type motorized spindle.

Number of pole-pairs	Calculation result (rpm)		Measured result (rpm)
	With MS	Without MS	
1	30336.12	34710.15	32400
2	30391.23	34710.15	
3	30487.51	34710.15	
4	30621.24	34710.15	

4. Discussion of the Calculation and Experimental Results

4.1. Validation of the Dynamic Model. Figure 5 shows the experimental vibration signals of the front end of spindle in y-direction with different speeds. When the rotational speed is 32400 rpm, the vibration value of the spindle is larger than other values with different speeds.

Figure 6 shows the experimental vibration displacement curve of the front end of the spindle rotor in y-direction. It can be found from the curve that the first critical speed of the system is about 32400 rpm.

To discuss the influence of the unbalanced magnetic force on the dynamic behaviors of the system, (12) was studied with and without the magnetic stiffness (MS). The first critical speeds of the spindle system obtained from calculation and experiment are listed in Table 2. As can be seen, considering the effect of MS, the calculated value of the first critical speed decreases and has an error of −6.37% compared with the experimental value. The difference in the first critical speeds between the two calculations is about 14.42%. The difference between the calculation and the measured result in this paper is within 7%, so the data in Table 2 can testify to the accuracy of the proposed dynamic model for motorized spindles. In addition, the calculated value of the first critical speed increases with the number of pole-pairs, which means the MS has a little influence on the system stability in multi-pole-pairs motors.

To study the influence of the MS more directly, the radial displacement of the rotor center is discussed and its value is $(x_r^2 + y_r^2)^{0.5}$. Figure 7 shows the theoretical radial displacements of the rotor center. When taking the MS into account, the vibration amplitudes in nonresonance and resonance regions increase; meanwhile the width of the speed region of high vibration amplitudes becomes larger. Combined with the analysis result from Table 2, it can be known that the MS reduces the system stability.

The influence of the radial displacement of the rotor center on the system stability is shown as in Figure 8. For the sake of discussion, the relative radial displacement of the rotor center e_c is taken and its value is $(x_r^2 + y_r^2)^{0.5}/e$. The larger the value of e_c is, the lower the critical speed of the system will be, and the downward trend is more gentle, which means when the critical speed of the spindle system is low, a little decrease of the critical speed would lead to more drastic whirling motion. Meanwhile, the ratio between the linear critical angular velocity ω_n and the nonlinear critical angular

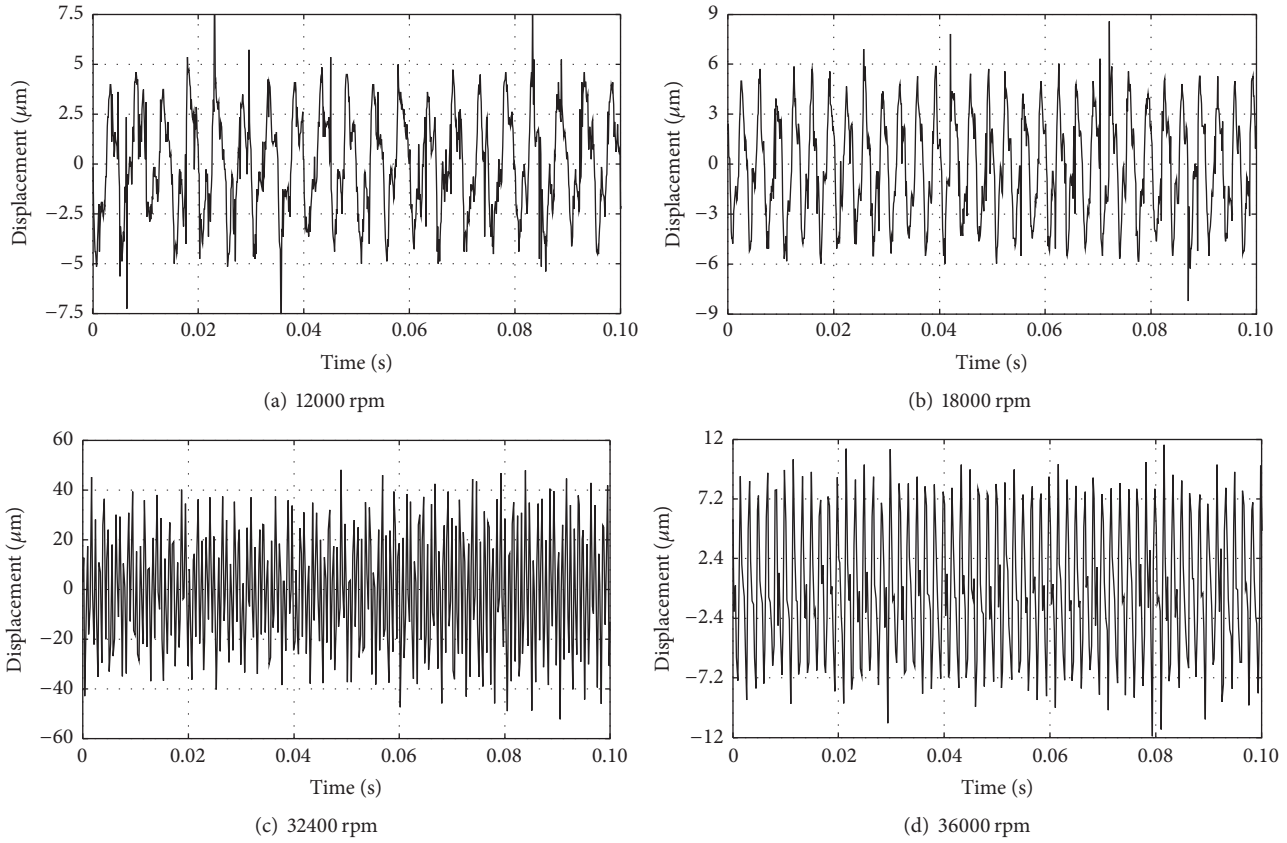

Figure 5: Experimental vibration signals of the front end of spindle in y-direction.

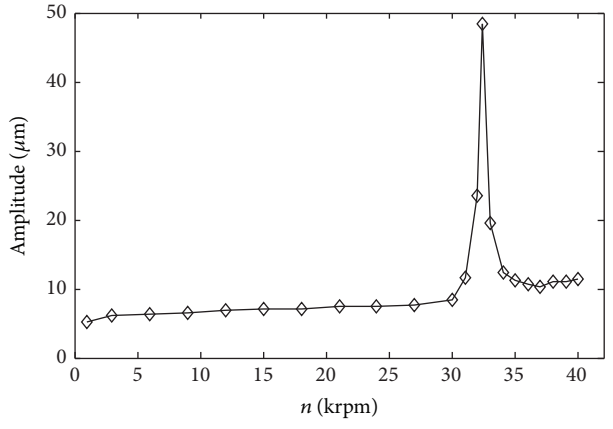

Figure 6: Experimental vibration displacement curve of the front end of spindle in y-direction.

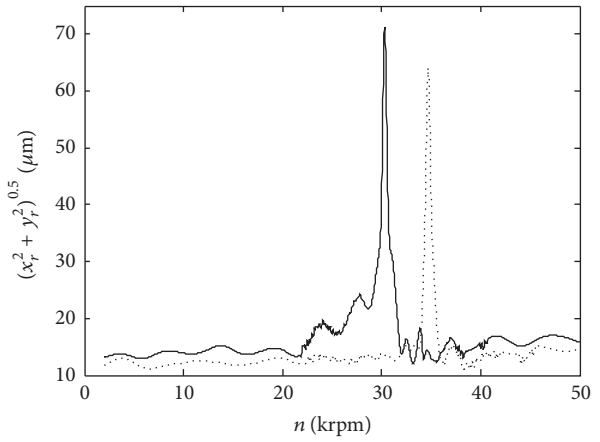

Figure 7: Theoretical radial vibration displacement curves of the rotor center.

velocity ω_c gently increases with the increasing of the value of e_c and then sharply decreases. Respectively, ω_n presents $[\{k_1 + k_2 + (K_{11} + K_{12} + K_{21} + K_{22})/4\}/m_r]^{0.5}$ [26] and ω_c is the angular velocity form of the first critical speed discussed in Table 2. In a significant extent of the value of e_c, the linear critical speed is about 0.65 times that of the nonlinear critical speed.

Figure 9 shows the Poincaré mapping of the rotor center in y-direction, which is a typical period-doubling bifurcation. When the angular velocity ω_f is at 3000 rad/s, there is a frequency division phenomenon in the system (Figure 9(a)); with the ω_f increase to 3180 rad/s, the chaos phenomenon occurs (Figure 9(b)), while the chaos disappears with the inverse bifurcation at 3300 rad/s.

4.2. Dynamic Design for Motorized Spindles. To instruct the dynamic design of the spindle system, the influence of system

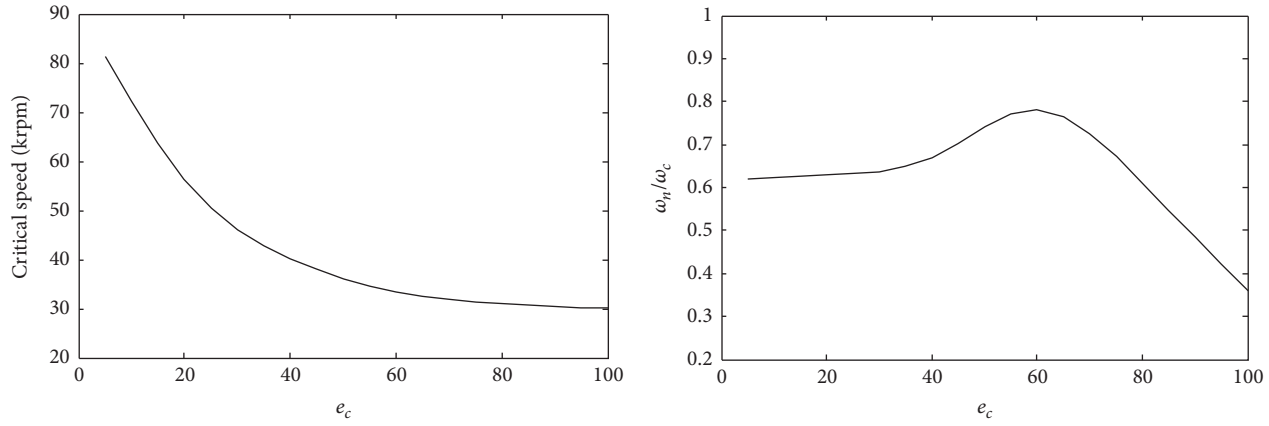

(a) Critical speed (b) Angular velocity ratio

Figure 8: Theoretical influence of the radial displacement of the rotor center on the system stability.

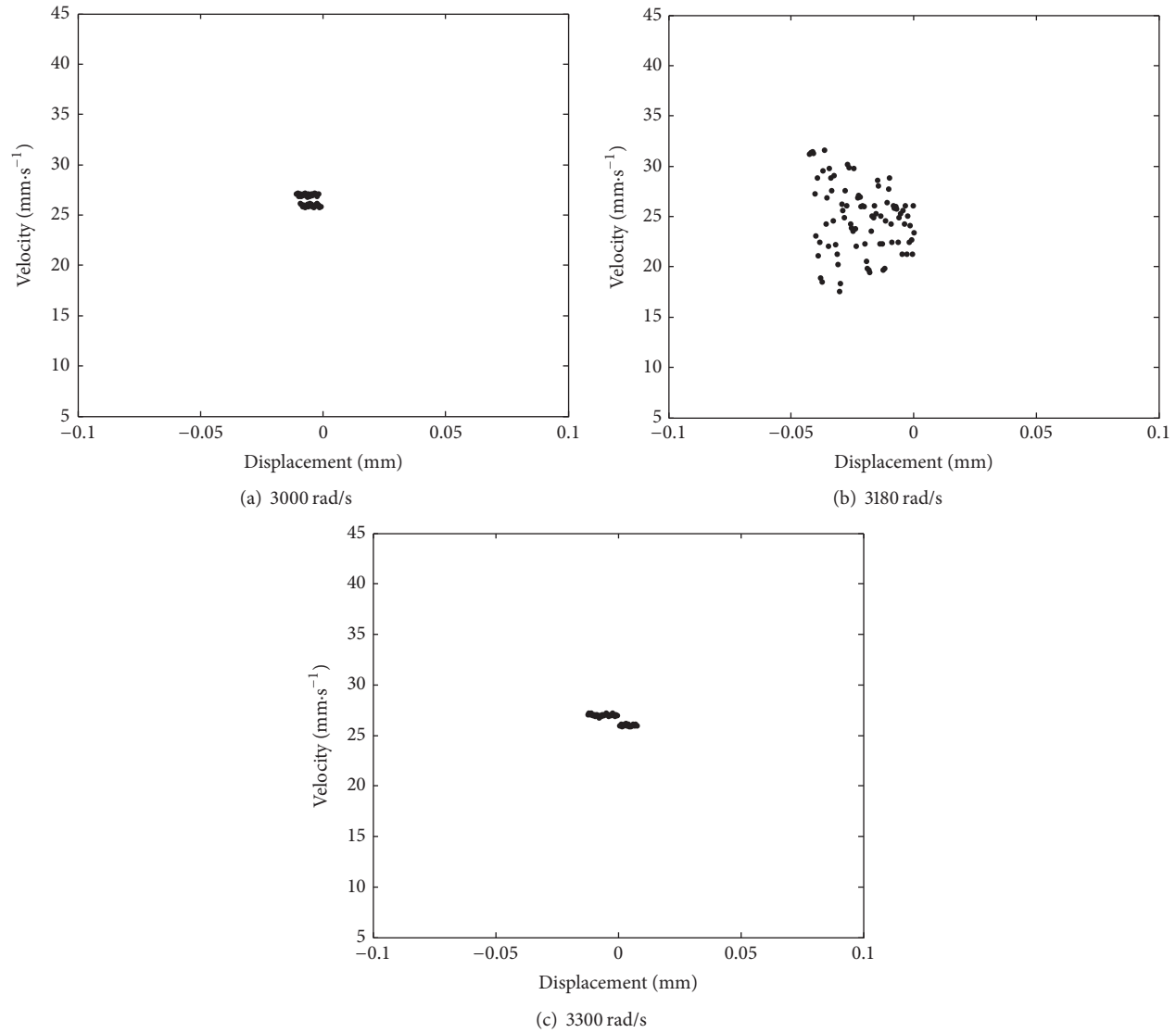

(a) 3000 rad/s (b) 3180 rad/s

(c) 3300 rad/s

Figure 9: Poincaré mapping of the rotor center in y-direction.

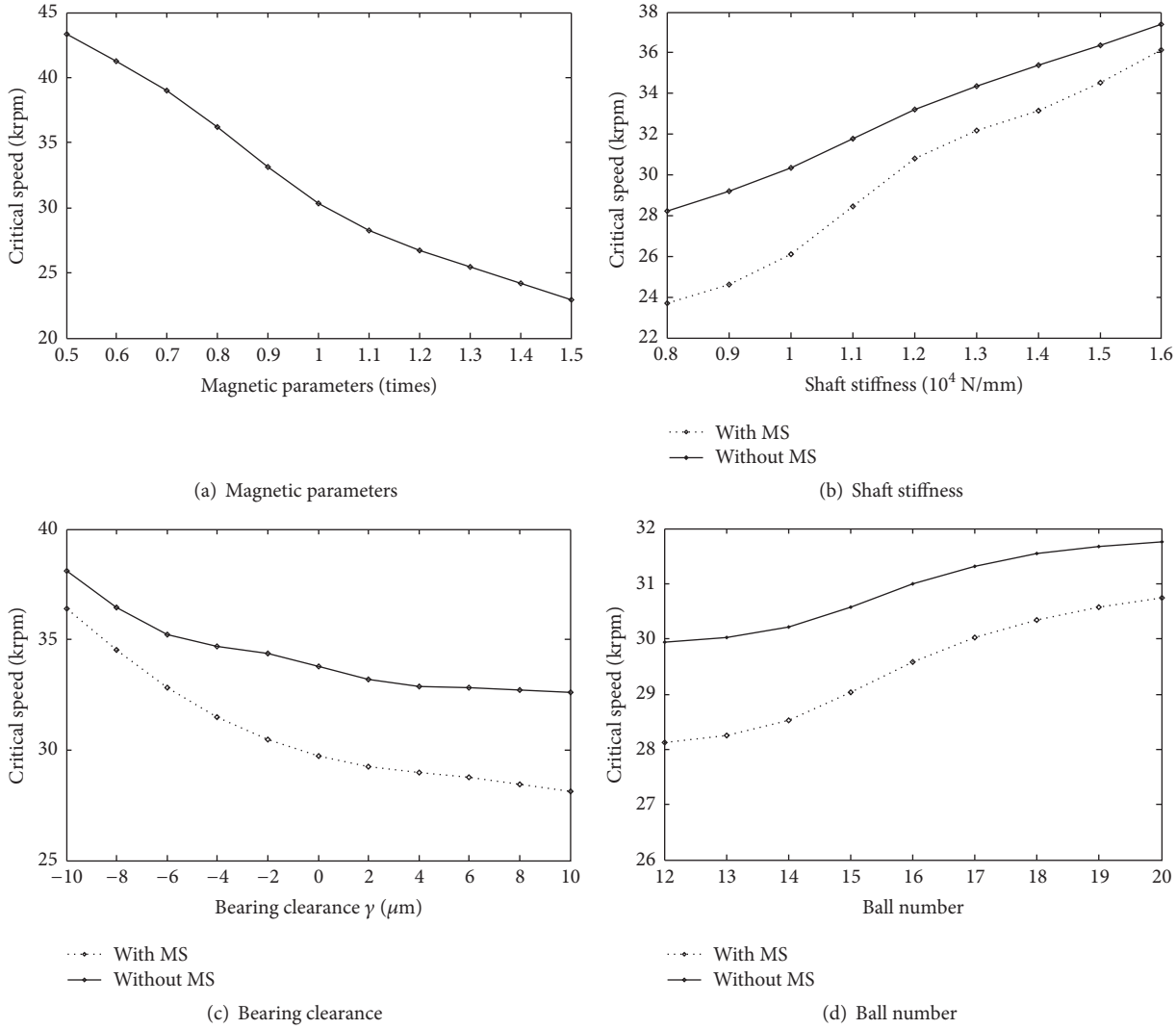

Figure 10: Theoretical influence of system parameters on critical speed.

parameters on the first critical speed is discussed and the theoretical results are shown as in Figure 10.

(a) The magnetic parameters present $R_g L_g \Lambda_0 / 2\sigma^2$ in Figure 10(a), and the unit of the abscissa is the multiple of $R_g L_g \Lambda_0 / 2\sigma^2$. With the increase of the inner radius of stator R_g and the effective length of rotor L_g and the decrease of uniform air gap δ_0, the critical speed decreases nonlinearly. When the magnetic parameters are 1.5 times that of the design value, the critical speed is close to the minimum rated speed. So the magnetic parameters are vital to the dynamic design of the spindle system, and their effects on the dynamic characteristic of motorized spindles cannot be ignored. Besides, the increase of the uniform air gap is of advantage to the rotor stability, but the gap cannot be too large and should be optimized.

(b) As shown in Figure 10(b), with the increase of the shaft stiffness, the first critical speed of the system increases, and the difference between the two calculations decreases, which means that high shaft stiffness can weaken the influence of the MS.

(c) Figure 10(c) shows the impact of the bearing clearance γ on the critical speed. Preload makes the bearing in a negative clearance state and improves the stability of the spindle system, which also can reduce the effect of MS.

(d) Figure 10(d) shows that the critical speed rises with the increase of ball number. This is because the increase of ball number leads to the improvement of the support stiffness and the frequency of the parametric vibration for ball bearings and meanwhile undermines the frequency multiplication and harmonic components of the parametric vibration, which benefits the stability of system. Without the consideration of the waviness on the race, the bearings which have more balls can effectively improve the operational stability of the spindle and decrease the influence of MS.

Based on the results of Figures 10(b), 10(c), and 10(d), it can be known that with the natural properties of the system increase, such as shaft stiffness and support stiffness, the influence of MS to the stability of the system decreases. That means the higher the stability of the system is, the lower the influence of MS to the stability of the system is.

5. Conclusions

This paper deals with the problem of analysing the dynamic behaviors of unbalanced high speed motorized spindles supported on ball bearings. An improved dynamic model which takes into account the unbalanced magnetic force is developed for the presented system. The model is studied by using the Lyapunov nonlinear vibration theory. Then, the validation test on a DX100A-24000/20-type motorized spindle is performed. From the calculated and experimental results the following conclusions are drawn.

(a) The proposed model accurately predicted the critical speed observed in the experiment and allows exploration of the magnetic force contribution within the context of its assumptions, which can be used for analysing the dynamic properties of high speed machine tool motorized spindle systems.

(b) The unbalanced magnetic force in the machine tool motorized spindle system increases the vibration response of the rotor and reduces the critical speed of the system. The influence of the MS on the stability of the system decreases with increasing the number of pole-pairs. With the increase of e_c, the critical speed of system decreases, while the ratio ω_n/ω_c increases and then sharply decreases. The period-doubling bifurcation occurs with the angular velocity ω_f being about 3200 rad/s.

(c) The system parameters greatly influence the critical speed of the system. The increase of the shaft stiffness and the ball number of bearings is of advantage to the stability, but the increase of the magnetic parameters and bearing clearance would lead to the decrease of the critical speed of the system. If the spindle system has higher natural properties, the influence of MS on the stability of the system will decrease.

Competing Interests

The authors declare that they have no competing interests.

Acknowledgments

This work was supported by National Natural Science Foundation of China (nos. 51405151 and 51005259).

References

[1] M. Munawar, J. C.-S. Chen, and N. A. Mufti, "Investigation of cutting parameters effect for minimization of sur face roughness in internal turning," *International Journal of Precision Engineering and Manufacturing*, vol. 12, no. 1, pp. 121–127, 2011.

[2] S.-T. Chen, K.-E. Chang, W.-P. Huang, H.-Y. Yang, and X.-M. Lee, "Development of a cost-effective high-precision bench machine tool for multi-level micro aspheric lighting-lens mold machining," *International Journal of Precision Engineering and Manufacturing*, vol. 13, no. 12, pp. 2225–2231, 2012.

[3] C.-W. Lin, "Simultaneous optimal design of parameters and tolerance of bearing locations for high-speed machine tools using a genetic algorithm and Monte Carlo simulation method," *International Journal of Precision Engineering and Manufacturing*, vol. 13, no. 11, pp. 1983–1988, 2012.

[4] T.-H. Duong, H.-C. Kim, D.-Y. Lee, S.-W. Lee, E.-S. Park, and T.-J. Je, "A theoretical deformation prediction of micro channels in ultra-precision machining," *International Journal of Precision Engineering and Manufacturing*, vol. 14, no. 2, pp. 173–181, 2013.

[5] S. Mohan, S.-H. Kweon, D.-M. Lee, and S.-H. Yang, "Parametric NURBS curve interpolators: a review," *International Journal of Precision Engineering and Manufacturing*, vol. 9, no. 2, pp. 84–92, 2008.

[6] R. Kurniawan and T. J. Ko, "A study of surface texturing using piezoelectric tool holder actuator on conventional CNC turning," *International Journal of Precision Engineering and Manufacturing*, vol. 14, no. 2, pp. 199–206, 2013.

[7] S. Jee and J. Lee, "Real-time inertia compensation for multi-axis CNC machine tools," *International Journal of Precision Engineering and Manufacturing*, vol. 13, no. 9, pp. 1655–1659, 2012.

[8] E. Abele, Y. Altintas, and C. Brecher, "Machine tool spindle units," *CIRP Annals—Manufacturing Technology*, vol. 59, no. 2, pp. 781–802, 2010.

[9] J. L. Dohne, T. D. Hinnerichs, J. P. Lauffer, C.-M. Kwan, M. E. Regelbrugge, and N. Shankar, "Active chatter control in a milling machine," in *Smart Structures and Materials: Industrial and Commercial Applications of Smart Structures Technologies*, vol. 3044 of *Proceedings of SPIE*, pp. 281–294, San Diego, Calif, USA, March 1997.

[10] B. Bossmanns and J. F. Tu, "A thermal model for high speed motorized spindle," *International Journal of Machine Tools & Manufacture*, vol. 43, no. 11, pp. 1163–1170, 1999.

[11] I. A. Zverev, I.-U. Eun, W. J. Chung, and C. M. Lee, "Simulation of spindle units running on rolling bearings," *The International Journal of Advanced Manufacturing Technology*, vol. 21, no. 10-11, pp. 889–895, 2003.

[12] L.-S. Law, J. H. Kim, W. Y. H. Liew, and S.-K. Lee, "An approach to monitoring the thermomechanical behavior of a spindle bearing system using acoustic emission (AE) energy," *International Journal of Precision Engineering and Manufacturing*, vol. 14, no. 7, pp. 1169–1175, 2013.

[13] M. Tiwari, K. Gupta, and O. Prakash, "Dynamic response of an unbalanced rotor supported on ball bearings," *Journal of Sound and Vibration*, vol. 238, no. 5, pp. 757–779, 2000.

[14] S. P. Harsha, "Nonlinear dynamic response of a balanced rotor supported by rolling element bearings due to radial internal clearance effect," *Mechanism and Machine Theory*, vol. 41, no. 6, pp. 688–706, 2006.

[15] J. Sopanen and A. Mikkola, "Dynamic model of a deep-groove ball bearing including localized and distributed defects—part 1: theory," *Proceedings of the Institution of Mechanical Engineers, Part K: Journal of Multi-body Dynamics*, vol. 217, no. 3, pp. 201–218, 2003.

[16] J. Sopanen and A. Mikkola, "Dynamic model of a deep-groove ball bearing including localized and distributed defects. Part 2: implementation and results," *Proceedings of the Institution of Mechanical Engineers, Part K: Journal of Multi-Body Dynamics*, vol. 217, no. 3, pp. 213–223, 2003.

[17] S.-H. Gao, X.-H. Long, and G. Meng, "Nonlinear response and nonsmooth bifurcations of an unbalanced machine-tool spindle-bearing system," *Nonlinear Dynamics*, vol. 54, no. 4, pp. 365–377, 2008.

[18] S.-H. Gao, X.-H. Long, and G. Meng, "Nonlinear response and stability of a spindle system supported by ball bearings," *Archive of Applied Mechanics*, vol. 80, no. 9, pp. 1069–1081, 2010.

[19] X. Chen, J. Liu, Y. He, P. Zhang, and W. Shan, "Thermal properties of high speed motorized spindle and their effects," *Journal of Mechanical Engineering*, vol. 49, no. 11, pp. 135–142, 2013.

[20] S. Y. Jiang and H. B. Mao, "Investigation of variable optimum preload for a machine tool spindle," *International Journal of Machine Tools & Manufacture*, vol. 50, no. 1, pp. 19–28, 2010.

[21] M. A. Alfares and A. A. Elsharkawy, "Effects of axial preloading of angular contact ball bearings on the dynamics of a grinding machine spindle system," *Journal of Materials Processing Technology*, vol. 136, no. 1–3, pp. 48–59, 2003.

[22] J. J. Qiu, *Electromechanical Analysis of Dynamics*, Science Press, Beijing, China, 1992.

[23] T. A. Harris, *Rolling Bearing Analysis*, John Wiley & Sons, New York, NY, USA, 4th edition, 2001.

[24] E. Kramer, *Dynamics of Rotors and Foundations*, Springer, New York, NY, USA, 1993.

[25] K. H. Shin, "On the performance of a single degree-of-freedom high-static-low-dynamic stiffness magnetic vibration isolator," *International Journal of Precision Engineering and Manufacturing*, vol. 15, no. 3, pp. 439–445, 2014.

[26] Z. Z. Li, D. Kong, Y. H. Jiao, Z. B. Chen, and M. Z. Li, "Nonlinear dynamics analysis on sealed rotor system," *Journal of Vibration and Shock*, vol. 28, no. 6, pp. 159–163, 2009.